Long tube flooding tests for investigating salt precipitation induced by CO_2 injection

Narayanan, Prinu; Khosravi, Maryam; Weibel, Rikke; Meirles, Leonardo Teixeira Pinto; Schovsbo, Niels Hemmingsen; Stenby, Erling H.; Yan, Wei

Published in:
Carbon Capture Science and Technology

Link to article, DOI:
10.1016/j.ccst.2023.100143

Publication date:
2023

Document Version
Publisher's PDF, also known as Version of record

Carbon Capture Science & Technology 9 (2023) 100143

Contents lists available at ScienceDirect

Carbon Capture Science & Technology

journal homepage: www.elsevier.com/locate/ccst

Full Length Article

Long tube flooding tests for investigating salt precipitation induced by CO_2 injection

Prinu Narayanan[a], Maryam Khosravi[a], Rikke Weibel[b], Leonardo Teixeira Pinto Meirles[c], Niels Hemmingsen Schovsbo[b], Erling H. Stenby[a], Wei Yan[a,*]

[a] Center for Energy Resources Engineering (CERE), Department of Chemistry, Technical University of Denmark (DTU), Denmark
[b] Geological Survey of Denmark and Greenland (GEUS), Denmark
[c] CERE, Department of Environmental and Resource Technology, DTU, Denmark

ARTICLE INFO

Keywords:
CO_2 storage
Depleted oil reservoir
Salt precipitation
Flooding Test
Simulation

ABSTRACT

Capturing a large amount of CO_2 from industry, energy production, or incineration plants and storing it in the subsurface such as depleted hydrocarbon reservoirs or saline aquifers can fundamentally reduce the footprint of atmospheric greenhouse gasses. Injection of CO_2 in a saline aquifer zone or depleted hydrocarbon reservoir will vaporize formation water and lead to potential salt precipitation in porous rock, thus increasing the risk of formation damage near the wellbore area and reducing the injectivity of CO_2 in the reservoir. Previous experimental studies on salt precipitation have focused on core flooding, including micro-core flooding, ordinary single-plug flooding, and composite core flooding. The length of the core plugs limits these flooding tests. They usually suffer from serious end effects, and it is generally challenging to investigate the variation along the flooding direction, especially after large pore volumes of injection. In this study (Project Greensand), we have researched and developed new equipment termed "long tube apparatus" to improve the understanding of salt precipitation and gage the effects of formation damage in detail for a North Sea depleted oil field reservoir (Nini West) under investigation, while injecting CO_2. The main aim of the experiment was to determine two properties such as salt and water content, which are used to evaluate the formation damage due to salt precipitation. Finally, a numerical simulation was carried out using CMG GEM in both 1D homogeneous model and another heterogeneous model honoring the channeling at the inlet. Results with qualitative agreement were achieved, especially with the heterogeneous model.

Introduction

To achieve the ambitious goal of carbon neutrality by 2050 set by the Danish government, CO_2 capture and storage (CCS) is considered a significant contributor to the portfolio of technologies for CO_2 emission reduction. Currently, geological storage of CO_2 in depleted oil/gas reservoirs or aquifers is being seriously investigated in Denmark. The phenomenon associated with salt precipitation can reduce the productivity in gas-producing fields (Kleinitz et al., 2003) or the injectivity in natural gas storage aquifers. The injection of CO_2 will result in water vaporization near the wellbore region and subsequently trigger salt precipitation inside the porous reservoir rock (Tang et al., 2015). The phenomena associated with salt precipitation further reduce porosity and permeability, thereby inducing formation damage and potentially decreasing the injectivity of CO_2 (André et al., 2011; Baumann et al., 2014; Peysson et al., 2014). The formation damage associated with CO_2 injection will depend on reservoir condition, fluid composition, injection rate, rock pore geometry, and mineralogy (Izgec et al., 2008). Reduction in CO_2 injectivity was observed in Snøhvit and Ketzin fields as part of carbon storage projects (Grude et al., 2014; Nooraiepour et al., 2018).

Several salt precipitation studies were carried out on a pore scale by using micromodel imaging and x-ray tomography in fully saturated brine (Kim et al., 2013; Norouzi Rad and Shokri, 2014; Miri et al., 2015; Berntsen et al., 2019; Falcon-Suarez et al., 2020; Akindipe et al., 2022) to determine the drying effects induced by CO_2 injection. Furthermore, core flooding experiments were carried out on ordinary single-plug to determine the drying process and the associated salt precipitation (Ott et al., 2011; Mahabadi et al., 2019). These flooding tests are limited by the length of the core plugs. They usually suffer from serious end effects (Andersen et al., 2017), and it is generally difficult to investigate the variation along the flooding direction, especially after large pore volumes of injection.

The slim tube test used in the oil industry influenced the long tube apparatus. The slim tube study experiment was carried out on an adequately pressure-rated steel tube pre-packed with glass beads or Ottawa sand with a length ranging from 40 to 80 ft. The test was carried out by saturating the slim tube with pressurized hydrocarbon oil at reser-

* Corresponding author.
E-mail address: weya@kemi.dtu.dk (W. Yan).

https://doi.org/10.1016/j.ccst.2023.100143
Received 25 July 2023; Received in revised form 15 September 2023; Accepted 16 September 2023

Nomenclature

Cont.	Content
Dep.	Deposited
Vap.	Vaporized
Dis.	Displaced
Red.	Reduced

voir temperature, followed by gas injection above the saturation pressure of the displacing fluid. The recovery of different injection pressures was plotted in a graph. The intersection of immiscible and miscible recoveries obtained during the slim tube study constitutes the Minimum Miscibility Pressure (MMP) data and is extensively used by reservoir engineers in the oil and gas industry (Yan et al., 2012; Ekundayo and Ghedan, 2013).

Similar to the slim tube design, we have designed a novel flooding test to investigate the salt precipitation effects in a long tube prefilled with sand particles. The long tube apparatus uses unconsolidated sand rather than core plugs and thus allows investigating the drying-out experiment on a larger scale which are historically unavailable for conventional core flooding experiments. Furthermore, it will enable a direct inspection and measurement of the properties at different tube positions through destructive testing after the flooding followed by the determination of water and salt contents. This allows a more detailed investigation of salt precipitation and the effects of formation damage.

This study evaluates the risks associated with salt precipitation when CO_2 is injected into a depleted hydrocarbon reservoir in the Nini Field in the Danish part of the North Sea. The long-tube experiment presented here provides a novel complementary method to the conventional core flooding method. In the following, we first present the sample and material used in the experiment, then the detailed design of the long-tube apparatus. After that, we present the experimental results for long-tube tests. Finally, we present the simulation analysis of the long-tube experiment using CMG GEM.

Rock, sand, and fluid properties

Rock samples properties

The Danish reservoirs are mostly composed of Cretaceous-Danian Chalk. However, the Siri Canyon formed in the Paleocene was eroded into the underlying Cretaceous-Danian Chalk Group and filled with Paleocene-Miocene hemipelagic and turbidities marls and mudstones interbedded with Paleocene-Eocene well-sorted, fine-grained glauconitic sandstones deposited from sandy mass flows and sandy turbidities (Petersen et al., 2022).

Core samples collected from well Nini 4 were first cleaned using the Soxhlet method and subjected to routine rock analysis. The obtained routine rock properties are displayed in Table 1. The poorly cemented sanstone was easily disintegrated into individual grains. The cleaned grains were then used for Experiments 2, 3, 4, and 5.

Sand properties

Two different types of sand has been used in this study: the Nini-4 sand and the BCS-315 quartz sand. The mineralogical composition of sandstones in the Nini-4 wells are shown in Fig. 1. They mainly consist of quartz and gluconitic clasts. on the other hand, BCS-315 quartz sand from Strobel Quarzsand GmbH (used as received) was procured from a third-party supplier with 99.1% of SiO_2, <0.1% of Fe_2O_3, and <0.2% of Al_2O_3 & TiO_2.

The grain size distribution of both Nini sand and BCS-315 was found to be similar. Hence, BCS-315 sand was used for the trial experiment (Experiment 1).

Details of grain size distribution between Nini-4 and BCS-315 sand can be found in Fig. 2.

Table 2
Synthetic brine composition that mimics formation water composition as recorded in produced water from the Nini field.

Element/Ion	Concentration (mg/l)
Na^+	29,300
K^+	211
Mg^{2+}	1027
Ca^{2+}	4800
Sr^{2+}	602
Ba^{2+}	123
Fe^{2+}	0.9
Cl^-	57,900
HCO^{3-}	100
SO_4^{2-}	6.3

Fluid properties

A synthetic brine was prepared by mimicking the produced water composition from the Nini field (Mohammadkhani et al., 2023; Schovsbo et al., 2023) and the exact composition details can be found in Table 2. The same synthetic brine was then used to perform Experiments 1, 3, and 4.

Long-Tube experiment

Experimental setup

As shown in Figs. 3 & 4, the long-tube experimental setup consists of a high-temperature oven, long-tube, high-pressure pumps, injection cylinders, accumulators, Back Pressure Regulator (BPR), temperature, and pressure sensors. Filters were used in the inlet and outlet of the long tube to ensure that the fluid flow was uniformly distributed. The key parameters used for the design of the Long-tube Flooding unit used in this study are provided in Table 3.

Experimental procedure

A long tube with 80 cm for vertical tubing and 600 cm for spiral tubing was pre-filled with unconsolidated sand. A sufficient volume of CO_2 was transferred from the 50 L cylinder to a portable laboratory cylinder by using the equilibrium method. A brief overview of the long tube experimental procedure can be viewed in Fig. 5.

The long tube was initially saturated with brine or deionized water and its pore volume (PV) was determined. CO_2 was used to displace brine or de-ionized water over a prolonged period, covering ~ 80 PV at a flow rate of 0.38, 0.75 and 1.5 cm^3/min. The experimental

Table 1
Routine rock properties of Nini-4 samples.

Sample Number	Well	Direction	Depth (m)	Gas Permeability (mD)	Grain Density (g/cm^3)	He Porosity (%)
94	Nini-4	Horizontal	1776.04	1190	2.70	35.4
96	Nini-4	Horizontal	1776.66	1420	2.69	34.6
97	Nini-4	Horizontal	1777.04	1230	2.70	35.5

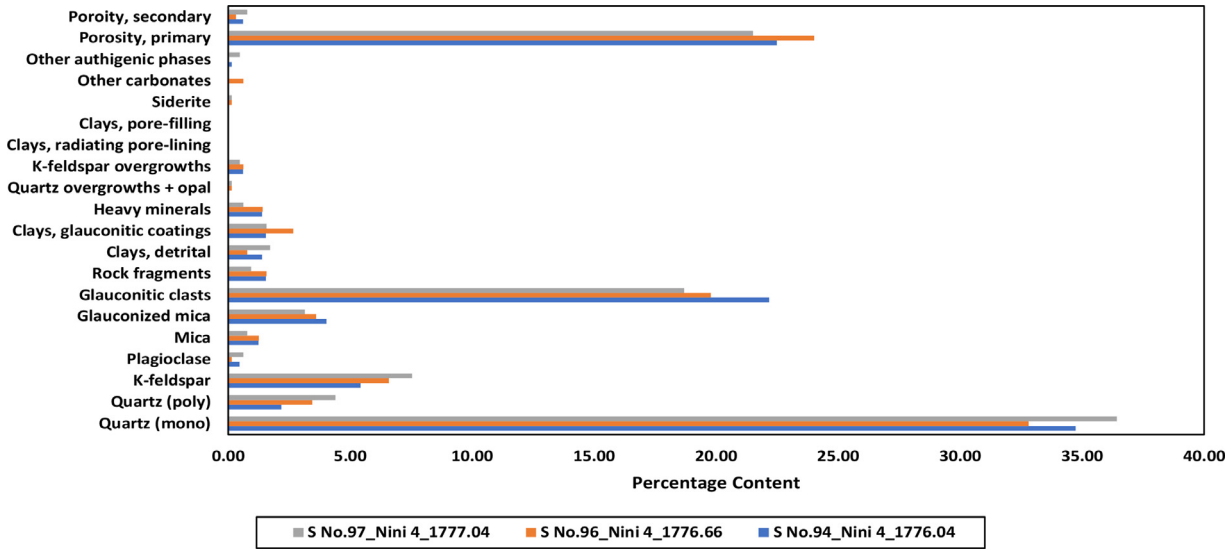

Fig. 1. Bulk mineralogical composition of the Nini samples.

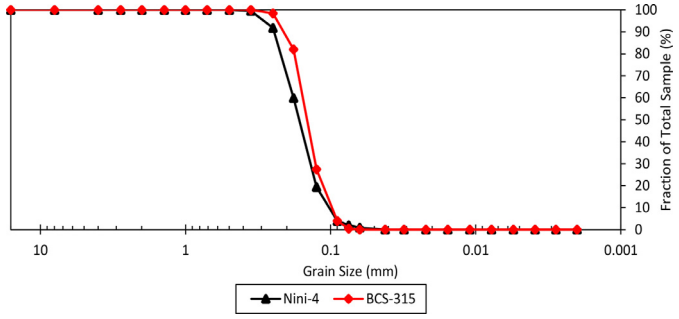

Fig. 2. Grain size distribution of Nini-4 and BCS-315 sand.

Table 3
Key parameters of long-tube apparatus.

Description	Values	Unit
Long Tube Material	Stainless steel	
Internal Diameter of Vertical Long-Tube	0.94	cm
Length of Vertical Long-Tube	80	cm
Vertical Long Tube Area	0.69	cm^2
Internal Diameter of Spiral Long-Tube	0.46	cm
Length of Spiral Long Tube	600	cm
Spiral Long Tube Area	0.16	cm^2
Injection Fluid	CO_2	n/a
Displacing Fluid	Brine/De-Ionized Water	n/a
CO_2 Viscosity at 60 °C and 200 bar	0.06	cP
Brine Viscosity at 60 °C and 200 bar	0.57	cP

geometry was vertical, and fluids were injected into the long tube by positive displacement pumps (ISCO pumps) at a constant rate. A back-pressure of 200 bar was set to control the outflow and stabilize the pressure during the experimental timeframe. The Joule-Thomson cooling effect was observed during the trial experiments by using CO_2 as the injecting fluid near to the BPR owing to the high permeability medium (Oldenburg, 2007). Henceforth, a series of accumulators were installed before the BPR to ensure that the Joule-Thomson cooling effect does not affect the flow regime during the experiment.

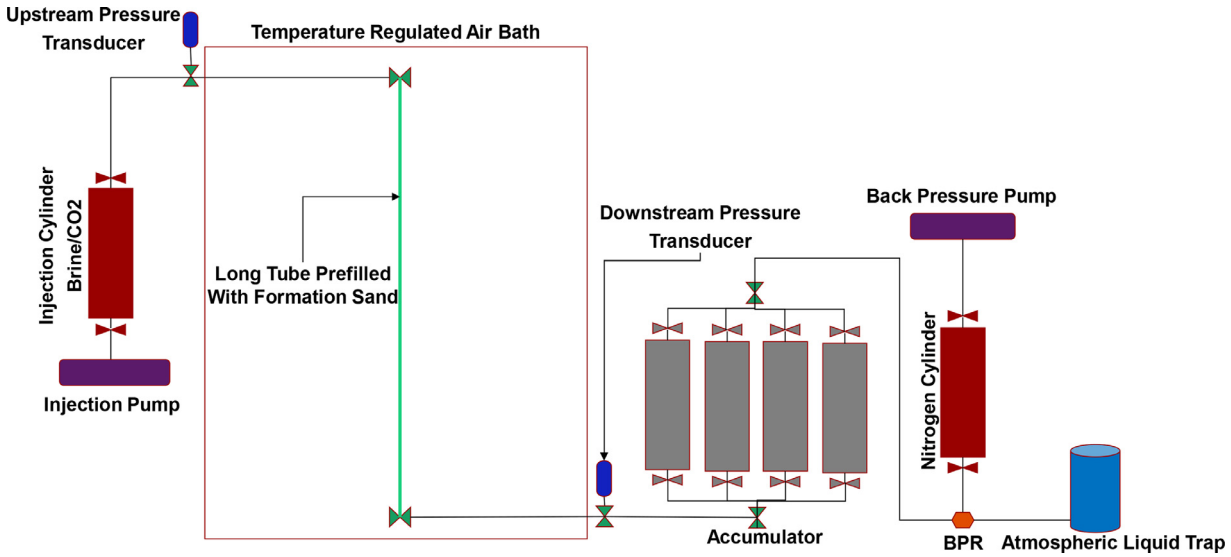

Fig. 3. Schematic of long tube apparatus with vertical tubing.

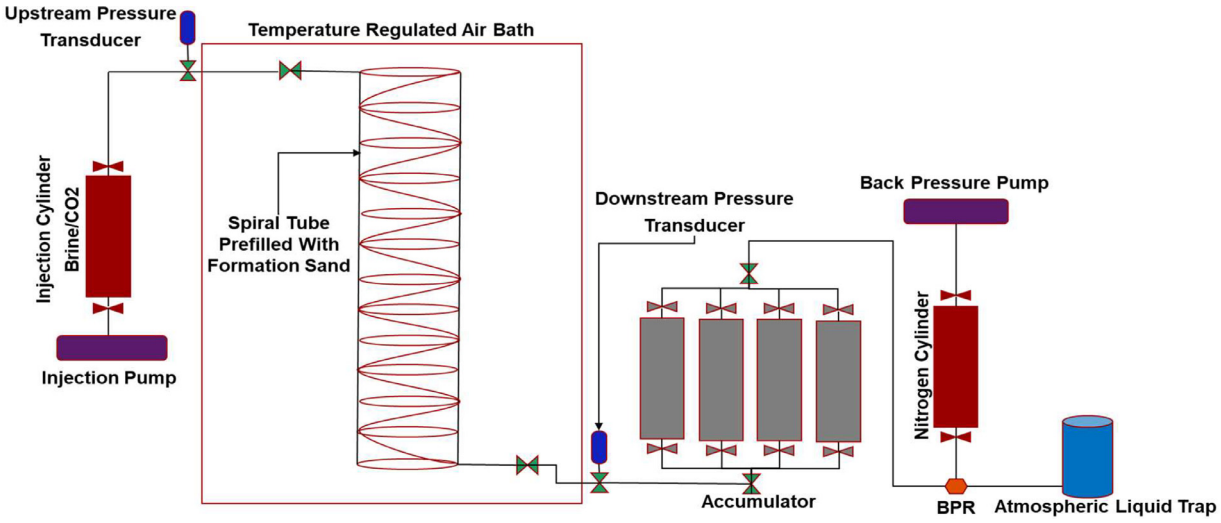

Fig. 4. Schematic of long tube apparatus with spiral tubing.

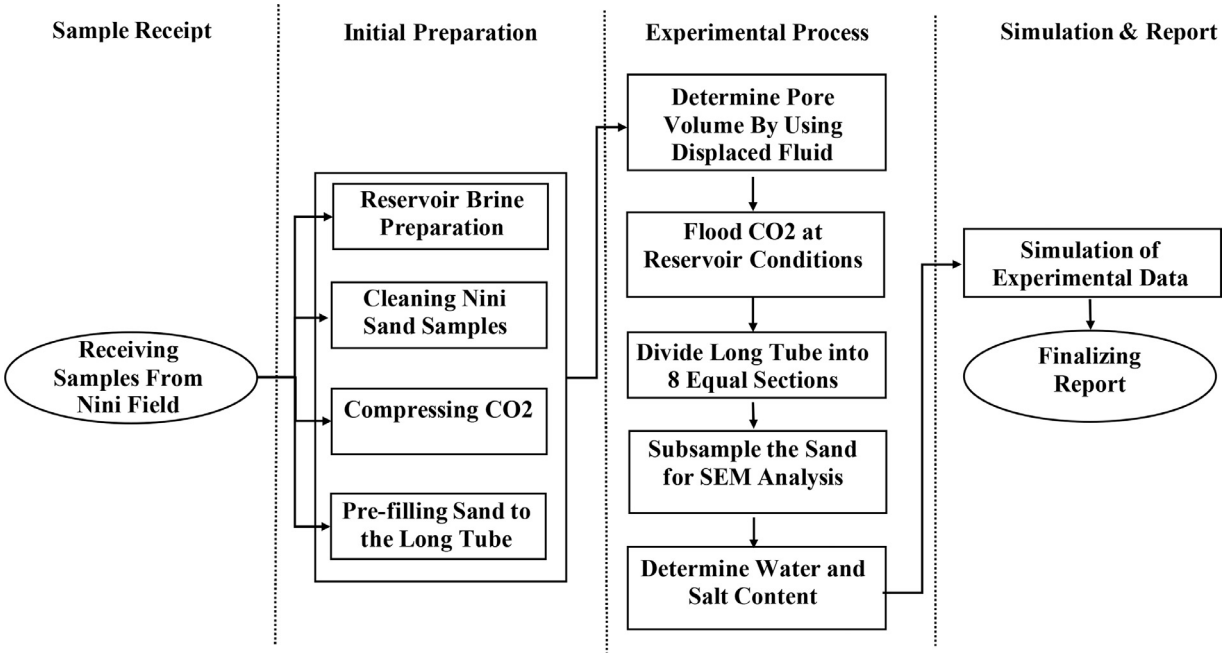

Fig. 5. Experimental flowchart.

After completion of the CO_2 flooding, the tube was retrieved from the flooding unit and subdivided into eight equal segments by using an appropriate cutting tool for stainless steel tubing. A sub-sample was collected from the top and bottom of each section to undergo SEM analysis. The remaining sand sample was collected in eight different beakers with appropriate weights recorded. The collected sand samples were used for a gravimetric methodology (Margolis et al., 2019) for water and salt content measurements. Using gravimetric methodology, de-ionized water was used as an effluent for determining salt content. The experimental results were then used for simulation. Details of simulation data can be found in Section 5.

Experimental results

Five experiments were carried out using the long-tube flooding unit at reservoir conditions (60 °C and 200 bar). A summary of experimental conditions can be found in Table 4, followed by a summary of water and salt content in Figs. 6 and 7 respectively.

Experiment 1 (BCS-315 & synthetic brine)

A trial experiment with the BCS-315 quartz sand was carried out before the actual experiment with reservoir sand, owing to its limited availability. The information and learnings gained during the trial experiments were incorporated for the real experiment with the reservoir sand and formation brine. After the first flooding experiment was completed, the tube was divided into eight segments with a length of 10 cm each.

Based on the close evaluation of each segment, it was observed that sand consolidation had occurred due to the presence of water, predominantly in the first section of the tubing resulting in the aggregation of

Table 4
Summary of experimental conditions.

Exp No.	Experimental Type	Long Tube Length (cm)	Flowrate (cm^3/minute)	Measured PV	PV Injected
1	BCS-315 & Synthetic Brine	80	1.50	19.89	47.53
2	Nini-4 Sand & Deionized Water	80	1.50	29.15	74.72
3	Nini-4 Sand & Synthetic Brine	80	1.50	29.42	81.68
4	Nini-4 Sand & Synthetic Brine	80	0.75	29.37	79.54
5	Nini-4 Sand & Synthetic Brine	600	0.38	49.50	80.15

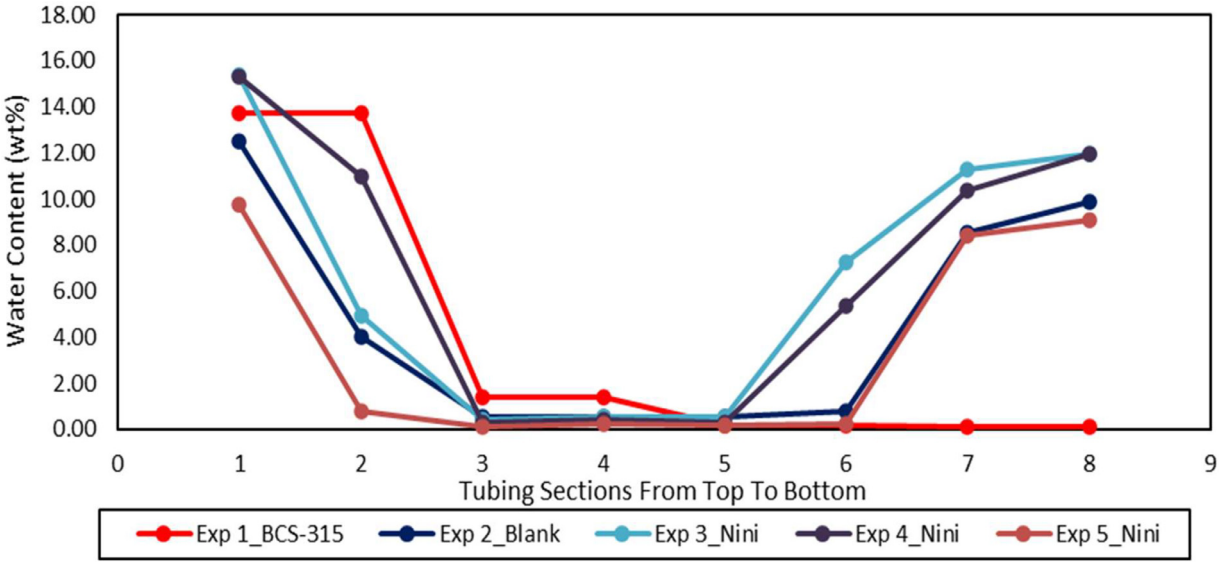

Fig. 6. Summary of water content.

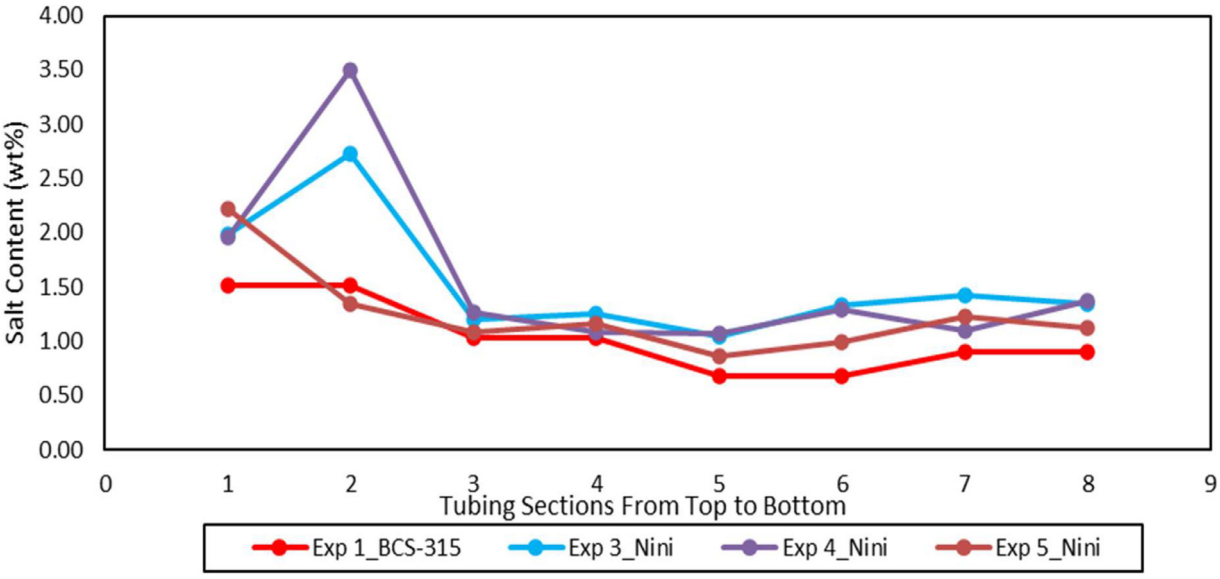

Fig. 7. Summary of salt content.

the former unconsolidated sandstones corroborating with quantitative analysis by gravimetric methodology (Fig. 8 and Table 5).

The consolidation phenomenon could be due to either one or a combination of several mechanisms as below;

(1) Increased salt precipitation due to the evaporation of water from the brine caused by CO_2 injection.
(2) Brine returns to the displaced segment or dried-out region owing to the capillary force.
(3) Enhanced water evaporation from near polycrystalline aggregate due to enhanced surface area and self-enhancing effect.
(4) Channeling of displacing fluid (CO_2) over displaced fluid (brine or de-ionized water) (Bacci et al., 2013).

The complete evaporation of water in the middle zone and subsequent salt precipitation did not lead to any blockage or reduction in permeability.

Table 5
Sand consolidation on the tubing segments for experiment 1.

		Long Tube Sections of 10 cm each from Top to Bottom							
Exp No.	Experimental Type	1	2	3	4	5	6	7	8
1	BCS-315 & Syntehtic Brine	Yes	Yes	No	No	No	No	No	No

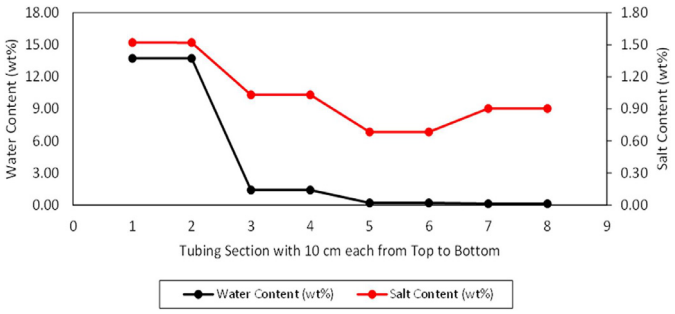

Fig. 8. Summary of water and salt content for experiment 1.

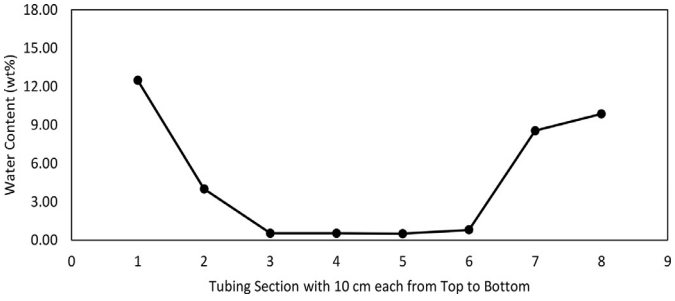

Fig. 9. Summary of water content for experiment 2.

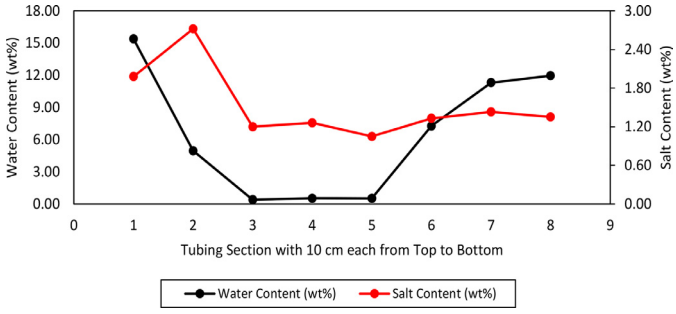

Fig. 10. Summary of water and salt content for experiment 3.

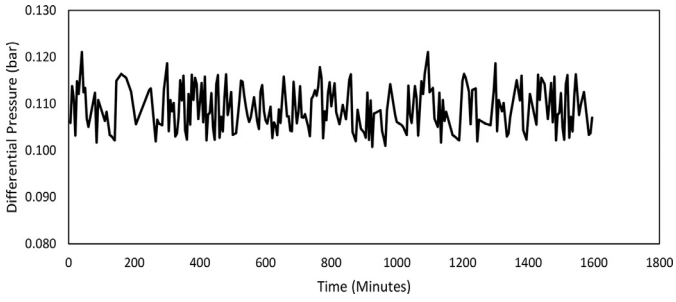

Fig. 11. Differential pressure data for experiment 3.

Experiment 2 (Nini-4 sand & deionized water)

To understand the consolidation process on the first flooding in detail and test the above hypothesis, a blank experiment was performed to determine the interaction between the injecting (CO_2) and displaced fluid (de-ionized water). Like the first experiment, all the relevant properties were measured except salt content (Fig. 9). Consolidation was observed for the first, second, seventh, and eighth section of this test, suggesting that aggregation of sand is not merely due to salt precipitation (Table 6).

Experiment 3 (Nini-4 sand & synthetic brine)

Based on the understanding from the first two experiments, a representative filling material (reservoir sand) and saturating fluid (formation brine) were used for the third experiment at reservoir conditions. CO_2 was then used as the displacing fluid, injected at 1.5 cm^3/minute over a period of 81.68 PV. Differential pressure data was recorded (Fig. 10) during the experiment and no significant decrease or increase in data was observed. Upon completion of the flooding experiment, the long tube was divided into 8 segments and the information on the segment consolidation can be viewed in Table 7. Unlike the 1st trial experiment associated with BCS-315, the consolidation was not limited to 1st & 2nd segments, instead, it was observed at the tail end of the tube covering the 6^{th}, $7^{th,}$ and 8^{th} (Fig. 11).

After completing the CO_2 flooding experiment, a sub-sample from each section (both top and bottom) of the tubing was collected and underwent SEM analysis, where a petrographical investigation was performed on platinum-coated rock chips using a Zeiss Sigma 300 VP field emission Scanning Electron Microscope (SEM) at 15 kV and 40–100 nA.

Table 6
Sand consolidation on the tubing segments for experiment 2.

		Long Tube Sections of 10 cm each from Top to Bottom							
Exp No.	Experimental Type	1	2	3	4	5	6	7	8
2	Nini-4 Sand & Deionized Water	Yes	Yes	No	No	No	No	Yes	Yes

Table 7
Sand consolidation on the tubing segments for experiment 3.

		Long Tube Sections of 10 cm each from Top to Bottom							
Exp No.	Experimental Type	1	2	3	4	5	6	7	8
3	Nini-4 Sand & Synthetic Brine	Yes	Yes	No	No	No	Yes	Yes	Yes

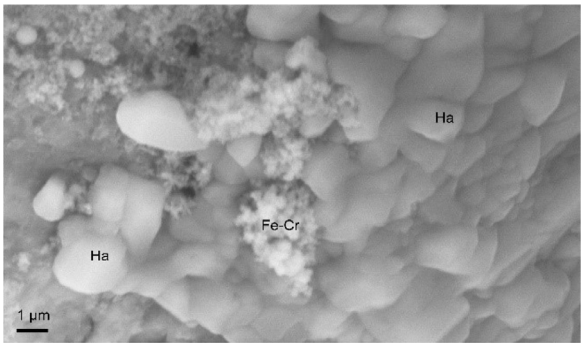

Fig. 12. SEM image of Section 1-top.

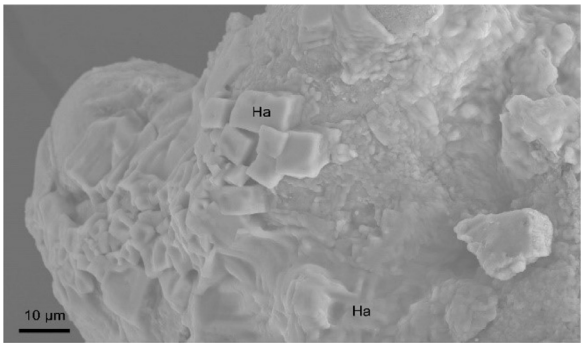

Fig. 13. SEM image of Section 2-top.

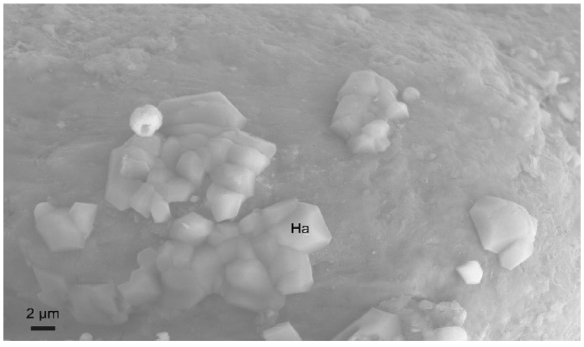

Fig. 14. SEM image of Section 4-top.

The chemical composition of the investigated minerals was obtained by Energy Dispersive Spectroscopy (EDS).

Figs. 12–15 provide the SEM images of the samples from Experiment 3. Halite (Ha) is precipitated from brine and Fe-Cr precipitates (Fe-Cr) are probably the result of dissolution of steel during the experiment.

From the SEM analysis, it was observed that halite was the most common mineral formed during the flooding experiment. Halite was precipitated as scattered tiny crystals and occasionally as patchy coatings with squared terminations. Halite was found to be predominant in the top and bottom of the long tube.

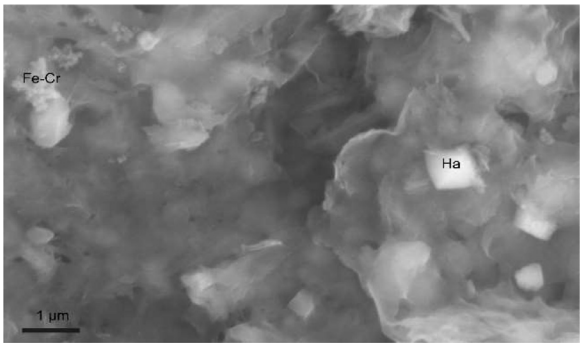

Fig. 15. SEM image of Section 8-bot.

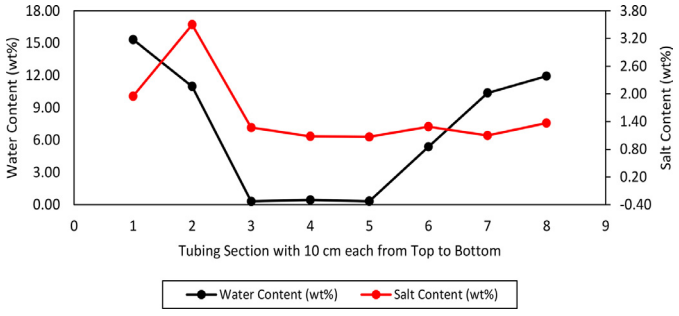

Fig. 16. Summary of water and salt content for experiment 4.

Experiment 4 (Nini formation sand & synthetic brine)

The flow rate was reduced from 1.5 to 0.75 cm^3/min for the fourth experiment to determine the impact on salt precipitation. The result (Table 8 and Fig. 16) after flooding with CO_2 as part of Experiment 4 was comparable with Experiment 3.

Experiment 5 (Nini formation sand & synthetic brine)

The fifth experiment was carried out by using spiral tubing with 600 cm in length. The fifth experiment was performed in order to compare the salt and water content from the previous four experiments performed with vertical tubing length of 80 cm.

The experimental results from Experiment 5 (Table 9 and Fig. 17) on the spiral tube were found to be comparable with previous vertical tube experiments (i.e. 1, 2, 3 & 4).

Observations and findings from the long-tube experiment

This study has resulted in the following important observations and findings:

- The long tube flooding apparatus developed here is an effective and complementary method to conventional core flooding to study salt precipitation during CO_2 injection. The method removes the limitation on the flooding length and provides more insightful results on water and salt distribution after flooding.
- The SEM analysis indicated the presence of halite in each section of the tubing.

Table 8
Sand consolidation on the tubing segments for experiment 4.

		Long Tube Sections of 10 cm each from Top to Bottom							
Exp No.	Experimental Type	1	2	3	4	5	6	7	8
4	Nini-4 Sand & Synthetic Brine	Yes	Yes	No	No	No	Yes	Yes	Yes

Table 9
Sand consolidation on the tubing segments for experiment 5.

		Long Tube Sections of 75 cm each from Top to Bottom							
Exp No.	Experimental Type	1	2	3	4	5	6	7	8
5	Nini-4 Sand & Synthetic Brine	Yes	Yes	No	No	No	No	Yes	Yes

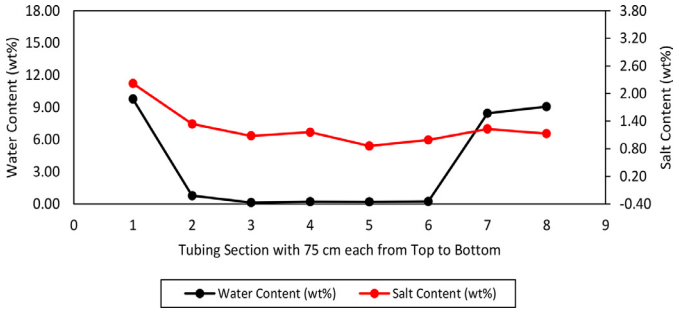

Fig. 17. Summary of water and salt content for experiment 5.

- Based on the gravimetric analysis, only the inlet and outlet showed relatively high-water saturation, and the water in the middle part was largely evaporated.
- A salt content larger than 1 wt% was observed throughout the tubing, but only the middle segments, where water is largely vaporized, have resulted salt in the deposited form.
- Consolidation of the packed sand was found in some segments close to the inlet and outlet, somewhat coinciding with the high water content regions.
- The results for the 80 cm tube and the 6 m tube are comparable in the water content, salt content, and consolidation observation.
- No significant increase in the pressure drop has been observed during the CO_2 flooding tests.

Simulation

Numerous modeling and simulations were carried out to identify the loss in injectivity owing to the salt precipitation associated with CO_2 injection near to wells (Giorgis et al., 2007; Muller et al., 2009; Kim et al., 2012; Tambach et al., 2015). In this study, a simulation was performed on vertical long-tube flooding using CMG GEM.

Simulation models

Two simulation models were built upon Experiment 3. The first simulation model was a 1D ***homogeneous model*** (1 × 1 × 80) as shown in Fig. 18(a). The second developed later, sought to rectify the limitations of the first model, by inserting some heterogeneity in different properties such as relative permeability set and well perforation locations (Fig. 18(b)). In the first model, an injection well was introduced at the uppermost grid and a producer at the lowermost grid. Relative permeability endpoints were adjusted such that ultimate remained water saturation at the bottom of the column could be matched. Based on water distribution at the end of experiments 2 and 3, several sensitivity analyses were conducted on the homogeneous model and finally, irreducible water saturation of 0.29 was chosen for the relative permeability curves with a Corey exponent of 3, which was suggested for loose sand packs in CMG-Builder. Table 10 provides detailed model specifications.

The second simulation model was constructed similarly to the first but a ***heterogeneous*** one (Fig. 18(b)). A new set of relative permeabilities was defined for the upper layers from 1 to 16, with larger irreducible water saturation. The injector well was perforated in the 17th grid block to mimic the channeling of CO_2 in the bypassed area in the inlet segment. Such treatment prevents CO_2 from entering the upper neighboring grids and thus keeps a relatively high water saturation in the area. The existence of such an area has been confirmed in experiments 1, 2, and 3. A simulation was then carried out on a homogenous model to set the appropriate permeability and capillary pressure, then switched to the heterogeneous model for detailed simulations.

To tune the interaction of water and CO_2, a binary interaction coefficient of 0.165 was selected. This choice allowed us to precisely align the

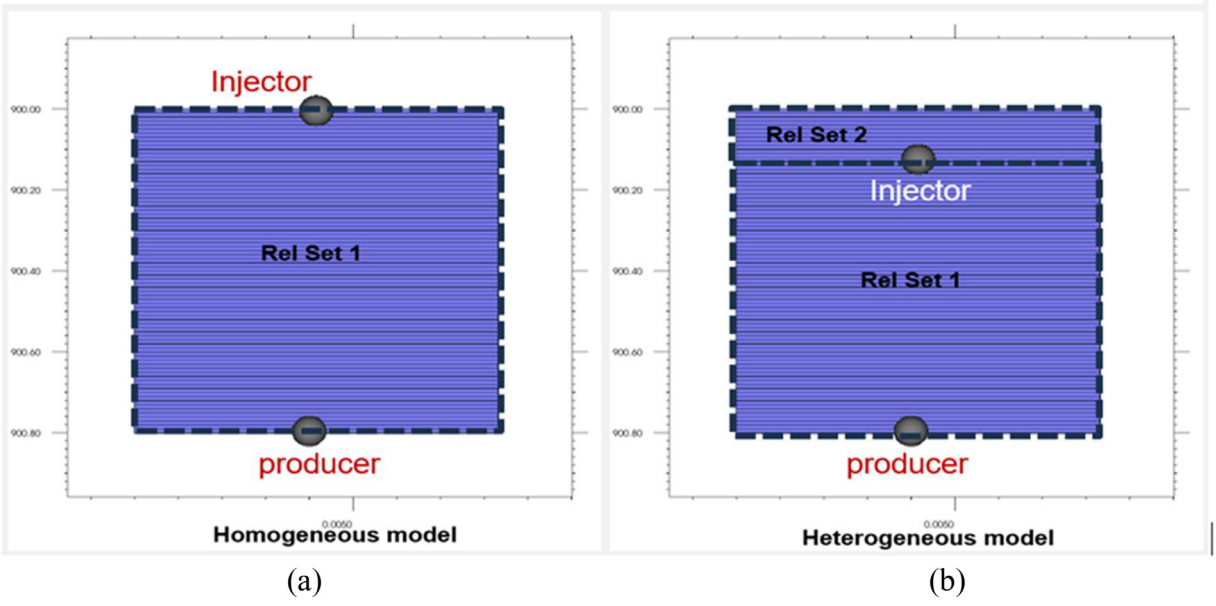

Fig. 18. Simulation models constructed for modeling CO_2 injection into a long vertical tube, (a) homogeneous model & (b) heterogeneous model.

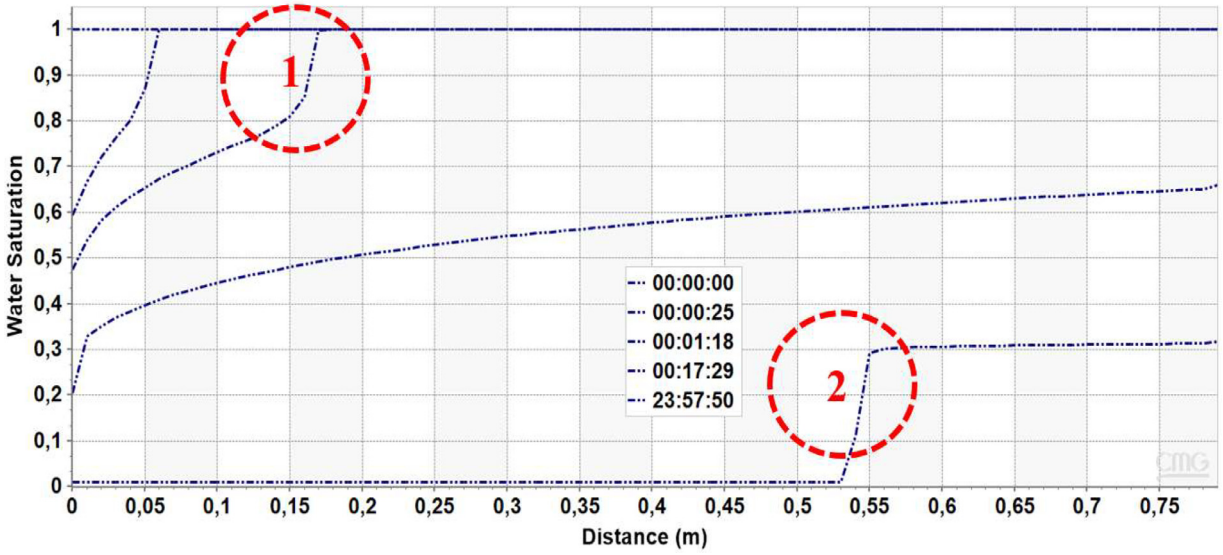

Fig. 19. Predicted water saturation distribution at different times within the linear path between the injector and producer in the homogeneous model.

Table 10
Simulation model specifications.

Description	Value	Unit
Length in x and y direction	0.0083	M
Length in z-direction	0.8	M
Porosity	52	%
Permeability	1578	mD
Temperature	60	°C
Pressure	200	Bar
Initial water saturation	100	%
CO_2 injection rate	0.0021	m^3/day
Irreducible water saturation in set number 1	0.29	
Irreducible water saturation in set number 2	0.45	
Water relative permeability at irreducible gas saturation	1	
Gas relative permeability at irreducible water saturation	1	
Exponent for calculation of k_r at different saturations of water and gas	3	

extension of the dried-out region with segment 6, ensuring a seamless match. Furthermore, to achieve the desired maximum salt deposition in segment 2, the diffusion coefficient of Na^+ and Cl^- was fine-tuned to a value of 4×10^{-6} cm^2/sec. Ion diffusion tends to homogenize the amount of salt deposition within the dried-out zone.

The PVT section of the model incorporates Peng-Robinson EOS with a 3-component system of components (CO_2, H_2O and a tracer of CH_4 for accuracy of calculations). The model accounted for both CO_2 dissolution (Harvey, 1996) and water vaporization (Canjar and Manning, 1967; Saul and Wagner, 1987).

The mineral dissolution and the precipitation reaction rate are calculated from Transient State Theory (TST) (Lasaga and Kirkpatrick, 1981). The equation for the TST rate is:

$$r = sgn\left[1 - \left(\frac{Q}{K_{eq}}\right)\right] \hat{A} S_w \left[k_0 + \sum_{i=1}^{n} k_i a_i^{wi}\right] \left|1 - \left(\frac{Q}{K_{eq}}\right)^{\xi}\right|^{\zeta} \quad (2)$$

$$\hat{A} = \hat{A}_0 \cdot \frac{N_m}{N_{mo}} \quad (3)$$

where Q is the activity product and K_{eq} is the chemical equilibrium constant. The $\hat{A}$ and $\hat{A}_0$ are the reactive surface area at the current time and at zero time respectively. N_m and N_{mo} are respectively the current moles of mineral and the moles of mineral at time zero. ξ *and* ζ are matching parameters. The rate constant k_0 at the current temperature, $T[K]$, can be calculated from rate constant k_0^* .

$$k_0 = k_0^* \exp\left[-\frac{E_a}{R}\left(\frac{1}{T} - \frac{1}{T^*}\right)\right] \quad (4)$$

where E_a is activation energy [J/mol] and R is the gas constant [8.314 J/mol K]. Halite equilibrium reaction with it's ions was modeled using the CMG-GEM database (GEOCHEM_V2):

$$\text{Halite}(\text{NaCl}) = Cl^- + Na^+ \quad (5)$$

For this reaction, a reactive surface area of 2163 m^2/m^3 was used with an activation energy of 7400 J/mol, and a Log10 reaction rate [mol/(m^2s)] of −0.21. These values were chosen based on the default recommendations of the CMG-GEM software. They can be derived from literature or used as matching parameters. However, the reported values in the literature can be accompanied by considerable uncertainties. In our simulations, the default values from CMG-GEM provided satisfactory results, thus we did not adjust them.

Typical water saturation profile

Fig. 19 shows the variation of water saturation along the porous media at different times. The displacement was primarily controlled by the Buckley-Leveret theory and gravity drainage, with the water at the top being displaced quickly in the beginning and the water saturation at the bottom staying high before the breakthrough. Two fronts could be identified by inspecting the water saturation profile. The first front (marked by "1") was the flooding front due to the viscous and gravity forces, and its movement was controlled by the predefined relative permeabilities. There was another dried-out front (marked by "2") lagging behind, with

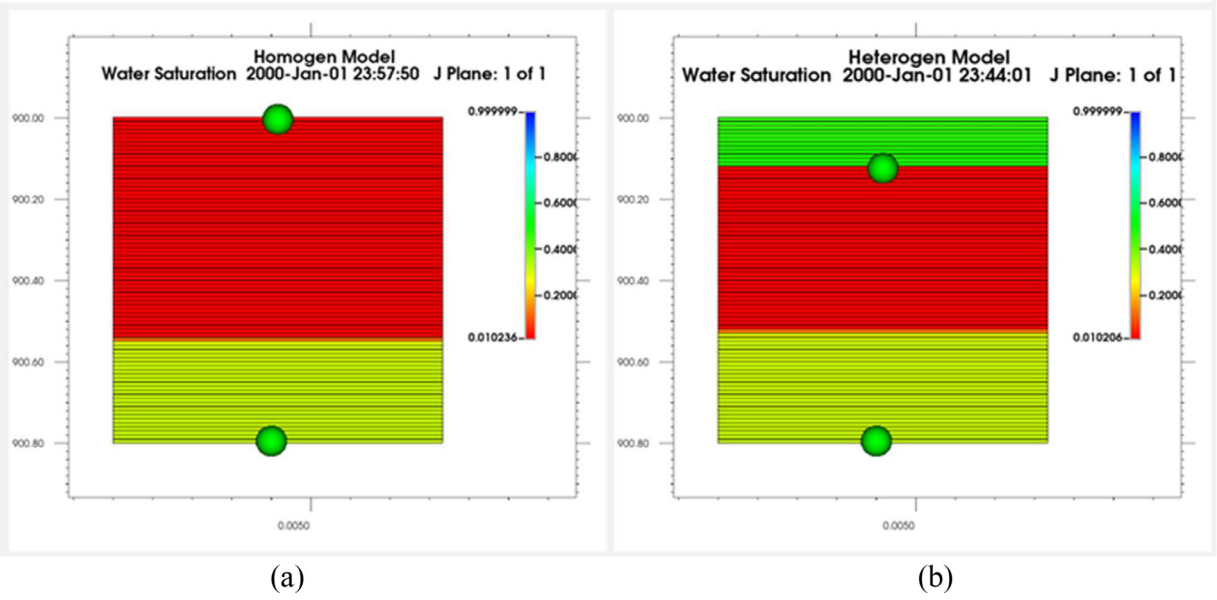

Fig. 20. Water saturation distribution in (a) homogeneous model and (b) heterogeneous model after 80 PV of CO_2 injection.

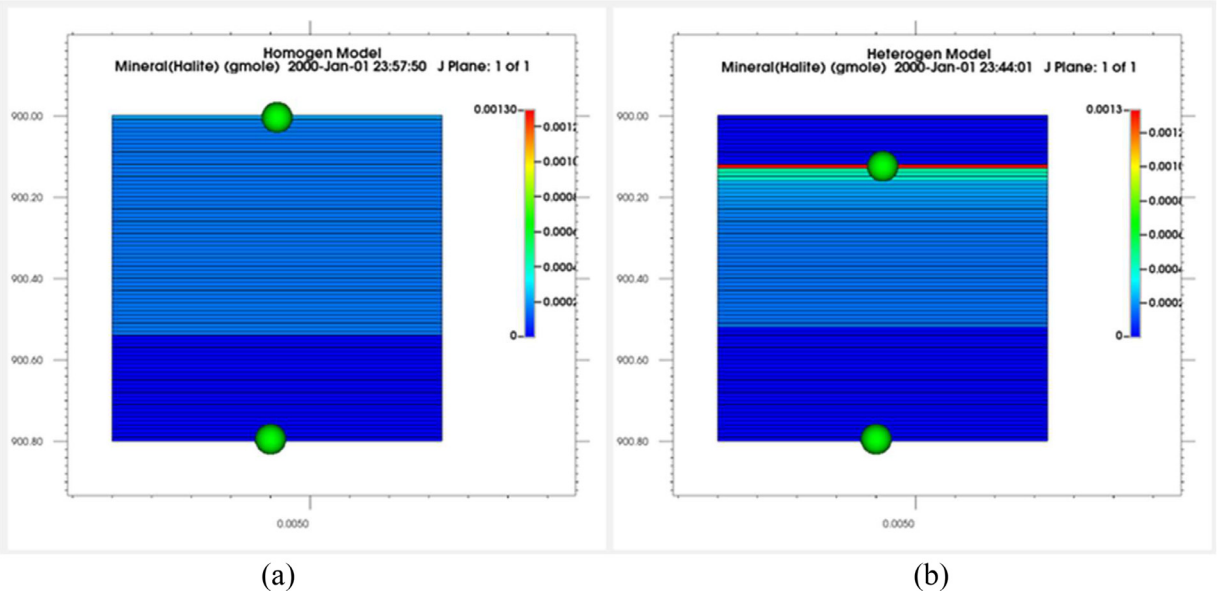

Fig. 21. Halite deposition distribution in (a) homogeneous model and (b) heterogeneous model after 80 PV of CO_2 injection.

the water saturation reduced to about 0.01 by vaporization. The flooding front moves much faster than the dried-out front. The brine phase between the two fronts appears stationary but was actually under the influence of two-phase flow and vaporization. The net outcome was an enrichment of the brine solution which led to salt precipitation at a later stage.

Comparison between experiment and simulation results

The experimental results are compared with the simulation results using two different models. Table 11 provides the water content, the salt content, and the deposited salt amount in each segment in experiment 3. Although the homogeneous model could capture the general production and deposition values, the detailed variations of saturation and deposition were described better with the heterogeneous model. Still, there was a gap between the predicted extent of dried-out regions and the experimental observation. The experimental dried-out front moves faster toward the producer, indicating a more significant amount of vaporized water and salt deposition. Previously, Khosravi et al. (2015) reported a similar scenario where the actual experimental vaporization rate was higher than the simulated results. It was attributed to spreading and Marangoni-induced turbulence, which increased the interfacial area between phases, and a similar phenomenon was evident for the long tube experiment.

Figs. 20 and 21 show the water and deposited salt distribution at the end of the flooding (after 80 PV injection), respectively. For the homogeneous model, salt deposition mainly occurred at the top, close to the injector, where the water saturation was low, and this contradicts the observation of high-water saturation close to the inlet. For the heterogeneous model, where a water region close to the inlet was deliberately

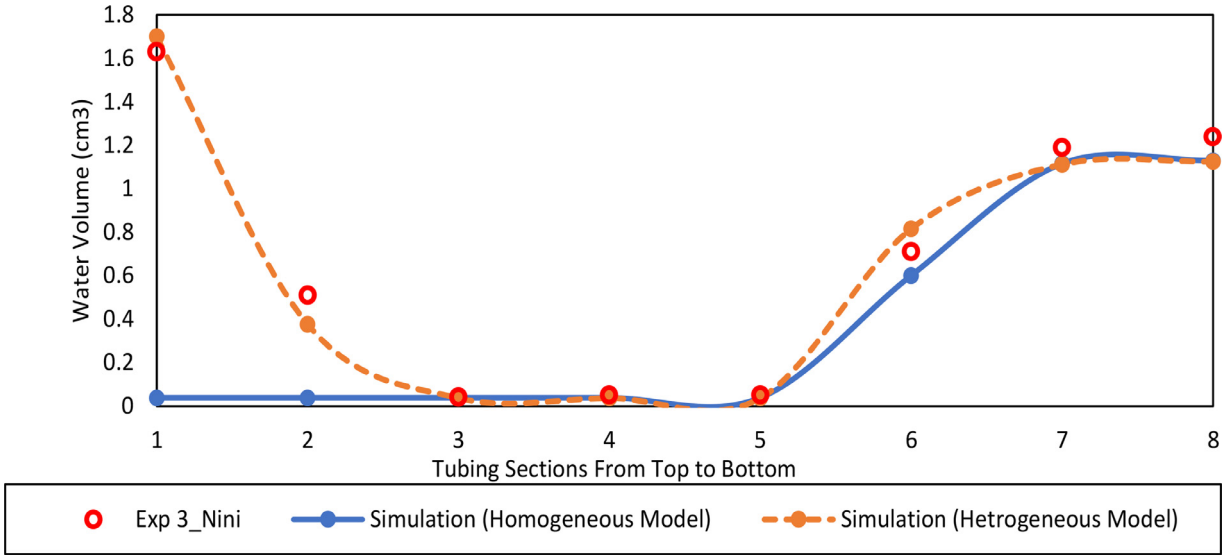

Fig. 22. Comparison of the experimental and simulated salt deposition along different segments of the sand-pack column, after 80 PV of CO_2 injection.

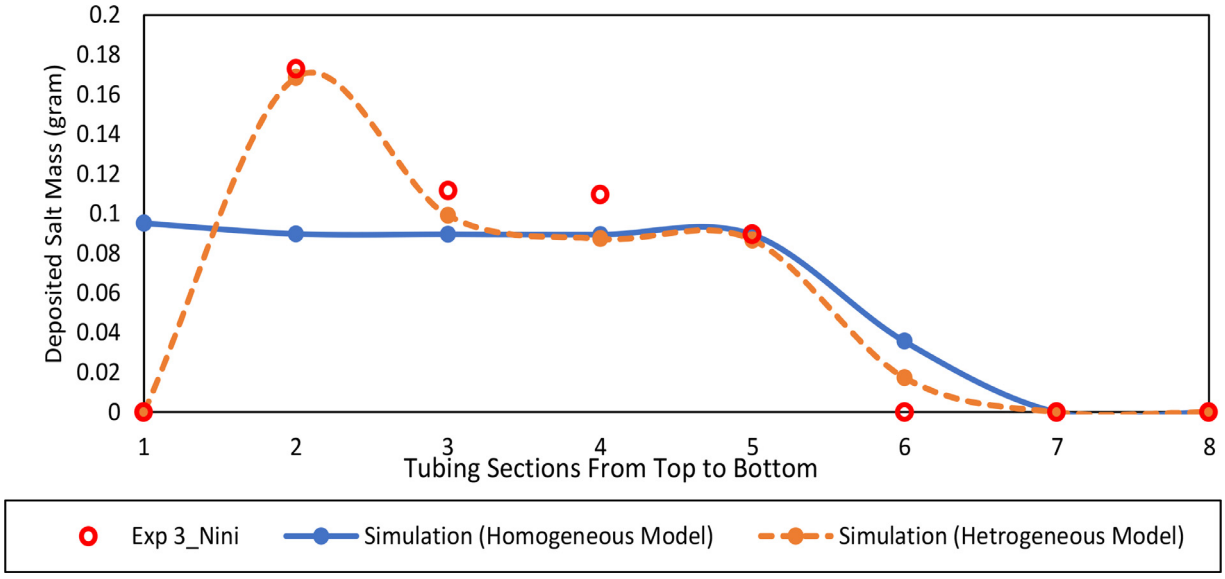

Fig. 23. Comparison of the experimental and simulated water content along different segments of the sand-pack column, after 80 PV of CO_2 injection.

Table 11
Comparison between the experimental and simulation results.

	Results of Experiment 3						Simulation (Homogeneous Model)		Simulation (Heterogeneous Model)	
Long Tube Sections	Water Cont. cm^3	Salt Cont. grams	Dep. Salt grams	Vap. Water cm^3	Red. Water cm^3	Dis. Water cm^3	Water Cont. cm^3	Dep. Salt grams	Water Cont. cm^3	Dep. Salt grams
1	1.63	0.21	-	-	2.00	2.00	0.04	0.0952	1.70	0.0000
2	0.51	0.28	0.1729	1.86	3.12	1.26	0.04	0.0898	0.38	0.2031
3	0.04	0.12	0.1116	1.2	3.59	2.39	0.04	0.0895	0.04	0.1018
4	0.05	0.12	0.1095	1.18	3.58	2.4	0.04	0.0894	0.04	0.0897
5	0.05	0.10	0.0895	0.96	3.58	2.61	0.04	0.0894	0.04	0.0892
6	0.71	0.13	-	-	2.92	2.92	0.60	0.0357	0.82	0.0178
7	1.19	0.15	-	-	2.44	2.44	1.12	0.0000	1.11	0.0000
8	1.24	0.14	-	-	2.39	2.39	1.13	0.0000	1.13	0.0000
Total	5.42	1.25	0.4834	5.19	23.58	18.39	0.04	0.0952	1.70	0.0000
% of Total Model				17.91	81.31	63.4				

bypassed, the simulation captures the high-water saturation in the upper segment as well as a high deposited salt content in the middle of the column.

The results of the heterogeneous model are in better agreement with the experimental observation. It can be hypothesized that certain compaction happened in the upper segments (the first segment and a part of the second one), which caused a change in the relative permeability curves and an increase in the irreducible water saturation. The injected gas bypassed this zone via a small channel and dried the segments below. Eventually, brine drained from the bypassed region under gravity into the dried-out segments just beneath it. The brine entering the new zone was quickly vaporized, resulting in salt deposition in the entry region. In the simulation with the heterogeneous model, the highest amount of salt deposition was obtained in the second segment. Fig. 21 also shows that the maximum salt deposition always happens in the first grid of the dried-out region no matter which model was used. The channeling in the heterogeneous model mainly moves the dried-out region deeper into the tube. In the dried-out region, the upper part had a higher salt deposition due to more exposure to dry injection gas.

Figs. 22 and 23 compare the experimental and simulated water content and deposited salt amount in each segment. The deposited salt amount was estimated using the total salt and saturated brine salinity. Fig. 22 shows that both models reasonably described the water content for segments 3 to 8. The major difference was that only the heterogeneous model could capture the high-water content close to the inlet. Similarly, Fig. 23 shows that the two models give similar deposited salt for segments 3 to 8, but only the heterogeneous model can capture the salt precipitation in the upper part (segments 1 and 2). In the homogeneous model, the salt precipitation in the inlet was relatively high. But a large amount of brine was bypassed and not vaporized close to the inlet in the heterogeneous model, which suppresses the salt precipitation.

Conclusions

Water vaporization associated with the huge amount of injected CO_2 can result in salt precipitation and even injectivity impairment in the near wellbore region. In this work, a new experimental method using a long tube with packed sand was developed to study salt precipitation on a larger scale as compared with the shorter lengths in conventional core floodings. After around 80 pore volumes of CO_2 injection, the tube was cut into 8 equal segments for different analyses, such as the water content, the salt content, and the SEM analysis. Compared to conventional flooding, the long-tube test provides more insight on the water and salt distribution in the porous media after the flooding. The SEM analysis clearly indicated the presence of halite in each section of the tubing. Only the inlet and outlet showed relatively high-water saturation, and the water in the middle part was largely evaporated. A salt content larger than 1 wt% was observed throughout the tubing, but only the middle segments deposited salt. Consolidation of the packed sand was found in some segments close to the inlet and outlet. No significant increase in the pressure drop has been observed after the CO_2 injection.

After the completion of experimental studies, a numerical simulation was carried out on the long-tube flooding results of experiment 3 using both a homogeneous model and a heterogeneous one. The typical salt-precipitation solution consists of two fronts: a leading front of immiscible displacement and a trailing front of vaporization, with the latter giving a dried-out zone, reflected in the simulation of the homogeneous model. In the homogeneous model, the salt deposition occurs mainly at the top, close to the injector where the water saturation was low, and this phenomenon contradicts our observation of high-water saturation close to the inlet. Hence, it was necessary to use a heterogeneous model, which can account for the bypassing of the brine close to the inlet, to capture the observed water and salt distribution. The heterogeneous model produces a dried-out zone in the middle of the tube and the highest amount of deposited salt in the upper part of this zone, which was in agreement with experimental results.

The long-tube flooding test provides a complementary approach to the conventional core flooding. It is recommended to adopt such a test in the laboratory investigation on salt precipitation. The current study is limited to one salinity and two flow rates. A wider range of conditions (temperature, pressure, salinity, and flow rate) should be investigated in the future. More tests with longer tubes can be conducted to determine the length effect and the optimal length. In the current long-tube flooding design as well as the conventional flooding design, the cross flow (perpendicular to the main displacement direction) from the neighboring region is not reflected. Since the capillary-driven cross flow is important to salt precipitation, it should be considered how to extend both flooding designs, which are essentially for one dimensional displacement, to honor this effect in a second dimension.

Declaration of Competing Interest

The authors declare that they have no known competing financial interests or personal relationships that could have appeared to influence the work reported in this paper.

Acknowledgement

This study was carried out as part of the “Project Greensand”, which aims to identify and mitigate risks associated with the development of the Nini West depleted oil field for CO_2 injection and storage. We would like to take this opportunity to acknowledge the funding provided by the Danish Energy Technology Development and Demonstration Programme (EUDP) and the European Union—NextGeneration EU. We also thank our industry partners Wintershall DEA and INEOS, and the software provider CMG.

References

Akindipe, D., Saraji, S., Piri, M., 2022. Salt precipitation in carbonates during supercritical CO_2 injection: a pore-scale experimental investigation of the effects of wettability and heterogeneity. Int. J. Greenhouse Gas Control 121, 103790.

Andersen, P.Ø., Standnes, D.C., Skjæveland, S.M., 2017. Waterflooding oil-saturated core samples-analytical solutions for steady-state capillary end effects and correction of residual saturation. J. Petroleum Sci. Eng. 157, 364–379.

André, L., Azaroual, M., Peysson, Y., Bazin, B., 2011. Impact of porous medium desiccation during anhydrous CO_2 injection in deep saline aquifers: up scaling from experimental results at laboratory scale to near-well region. Energy Procedia 4, 4442–4449.

Bacci, G., Durucan, S., Korre, A., 2013. Experimental and numerical study of the effects of halite scaling on injectivity and seal performance during CO_2 injection in saline aquifers. Energy Procedia 37, 3275–3282.

Baumann, G., Henninges, J., De Lucia, M., 2014. Monitoring of saturation changes and salt precipitation during CO_2 injection using pulsed neutron-gamma logging at the Ketzin pilot site. Int. J. Greenhouse Gas Control 28, 134–146.

Berntsen, A., Todorovic, J., Raphaug, M., Torsæter, M., Panduro, E.A.C., Gawel, K., 2019. Salt clogging during supercritical CO_2 injection into a downscaled borehole model. Int. J. Greenhouse Gas Control 86, 201–210.

Canjar, L.N., Manning, F.S., 1967. Thermodynamic Properties and Reduced Correlations For Gases. Gulf Publishing Co, Houston, TX.

Ekundayo, J.M., Ghedan, S.G., 2013. Minimum miscibility pressure measurement with slim tube apparatus-how unique is the value? In: Proceedings of the SPE Reservoir Characterization and Simulation Conference and Exhibition. OnePetro.

Falcon-Suarez, I.H., Livo, K., Callow, B., Marin-Moreno, H., Prasad, M., Best, A.I., 2020. Geophysical early warning of salt precipitation during geological carbon sequestration. Sci. Rep. 10 (1), 16472.

Giorgis, T., Carpita, M., Battistelli, A., 2007. 2D modeling of salt precipitation during the injection of dry CO_2 in a depleted gas reservoir. Energy Convers. Manage. 48 (6), 1816–1826.

Grude, S., Landrø, M., Dvorkin, J., 2014. Pressure effects caused by CO_2 injection in the Tubåen Fm., the Snøhvit field. Int. J. Greenhouse Gas Control 27, 178–187.

Harvey, A.H., May 1996. Semiempirical correlation for henry’s constants over large temperature ranges. AIChE J. 42, 1491–1494.

Izgec, O., Demiral, B., Bertin, H., Akin, S., 2008. CO_2 injection into saline carbonate aquifer formations I. Transp. Porous Media 72, 1–24.

Khosravi, M., Rostami, B., Emadi, M., Roayaei, E., 2015. Marangoni flow: an unknown mechanism for oil recovery during near-miscible CO_2 injection. J. Petroleum Sci. Eng. 125, 263–268.

Kim, K.Y., Han, W.S., Oh, J., Kim, T., Kim, J.C., 2012. Characteristics of salt-precipitation and the associated pressure build-up during CO_2 storage in saline aquifers. Transp. Porous Media 92, 397–418.

Kim, M., Sell, A., Sinton, D., 2013. Aquifer-on-a-Chip: understanding pore-scale salt precipitation dynamics during CO_2 sequestration. Lab Chip 13 (13), 2508–2518.

Kleinitz, W., Dietzsch, G., Köhler, M., 2003. Halite scale formation in gas-producing wells. Chem. Eng. Res. Design 81 (3), 352–358.
Lasaga, A., Kirkpatrick, J., 1981. Kinetics of Geochemical Processes. De Gruyter, Berlin, Boston.
Mahabadi, N., Dai, S., Seol, Y., Jang, J., 2019. Impact of hydrate saturation on water permeability in hydrate-bearing sediments. J. Petroleum Sci. Eng. 174, 696–703.
Margolis, S.A., Huang, P.H., Hădărugă, N.G., Hădărugă, D.I., 2019. Water determination. In: Encyclopedia of Analytical Science, pp. 382–390.
Miri, R., van Noort, R., Aagaard, P., Hellevang, H., 2015. New insights on the physics of salt precipitation during injection of CO_2 into saline aquifers. Int. J. Greenhouse Gas Control 43, 10–21.
Mohammadkhani, S., Olsen, D., Weibel, R., Fogden, A., Schovsbo, N.H., 2023. Evaluation of cyclic injection of supercritical Co_2 into a glauconitic sandstone reservoir a case study for Co_2 storage in the depleted Nini West Oil Field. Danish North Sea.
Muller, N., Qi, R., Mackie, E., Pruess, K., Blunt, M.J., 2009. CO_2 injection impairment due to halite precipitation. Energy Procedia 1 (1), 3507–3514.
Nooraiepour, M., Fazeli, H., Miri, R., Hellevang, H., 2018. Salt precipitation during injection of CO_2 into saline aquifers: lab-on-chip experiments on glass and geomaterial microfluidic specimens, pp. 21–26.
Norouzi Rad, M., Shokri, N., 2014. Effects of grain angularity on NaCl precipitation in porous media during evaporation. Water Resour. Res. 50 (11), 9020–9030.
Oldenburg, C.M., 2007. Joule-Thomson cooling due to CO_2 injection into natural gas reservoirs. Energy Convers. Manage. 48 (6), 1808–1815.
Ott, H., de Kloe, K., Marcelis, F., Makurat, A., 2011. Injection of supercritical CO_2 in brine saturated sandstone: pattern formation during salt precipitation. Energy Procedia 4, 4425–4432.
Petersen, H.I., Springer, N., Weibel, R., Schovsbo, N.H., 2022. Sealing capability of the Eocene–Miocene Horda and Lark formations of the Nini West depleted oil field–implications for safe CO_2 storage in the North Sea. Int. J. Greenhouse Gas Control 118, 103675.
Peysson, Y., André, L., Azaroual, M., 2014. Well injectivity during CO_2 storage operations in deep saline aquifers-Part 1: experimental investigation of drying effects, salt precipitation and capillary forces. Int. J. Greenhouse Gas Control 22, 291–300.
Saul, A., Wagner, W., 1987. International equations for the saturated properties of ordinary water substance. J. Phys. Chem. Ref. Data 16, 893–901.
Schovsbo, N.H., Holmslykke, H.D., Kjøller, C., Hedegaard, K., Kristensen, L., Thomsen, E., & Esbensen, K.H. Types of formation water and produced water in Danish oil-and gasfields: implications for enhanced oil recovery by 'smart'water injection. 2023
Tambach, T.J., Loeve, D., Hofstee, C., Plug, W.J., Maas, J.G., 2015. Effect of CO_2 Injection on brine flow and salt precipitation after gas field production. Transp. Porous Media 108 (1), 171–183.
Tang, Y., Yang, R., Du, Z., Zeng, F., 2015. Experimental study of formation damage caused by complete water vaporization and salt precipitation in sandstone reservoirs. Transp. Porous Media 107, 205–218.
Yan, W., Michlesen, M.L., Stenby, E.H., 2012. Calculation of minimum miscibility pressure using fast slimtube simulation. In: Proceedings of the SPE Improved Oil Recovery Symposium. OnePetro.